PtCu/Pt core/atomic-layer shell hollow octahedra for oxygen reduction and methanol oxidation electrocatalysis †

Yi Zhou, Qiang Yuan*

Experimental section

Chemicals

Platinum (II) acetylacetonate ($Pt(acac)_2$, 97%), copper (II) acetylacetonate ($Cu(acac)_2$, 97%), and cobalt (II) acetylacetonate ($Co(acac)_2$, 97%) were purchased from Sigma-Aldrich. Ascorbic acid (AA, 99.7%) was obtained from Kermel. Dodecyltrimethylammonium bromide (99%) and N, N-dimethylforma-mide (DMF, 99.8%) were obtained from Aladdin. Nitric acid (HNO_3, 65-68%) was purchased from Sinopharm Chemical Reagent Co. Ltd. (Shanghai, China). Pt/C (20 wt%) was purchased from Johnson Matthey. Vulcan XC-72 was purchased from Cabot. All chemicals were used as received without further purification treatment.

Synthesis of S-PtCuCo OHs：

In a typical synthesis, 4.0 mg $Pt(acac)_2$, 20 mg AA and 28 mg dodecyl trimethyl ammonium bromide was dissolved in 12 mL Teflonlined autoclave containing 4.9 mL DMF. Then, adding 2 mL 0.25 M $Cu(acac)_2$ (dissolved in DMF) and 0.1 mL 0.1 M $Co(acac)_2$ (dissolved in DMF) in the mixed solution. The resulting mixture was magnetically stirred at room temperature for 20 min and heated at 180 °C for 24 hours. The as obtained product was centrifuged three times at 10000 rpm for 20 min with ethanol, and the final product was stored in 5 mL ethanol solution.

Synthesis of S-PtCu OHs：

4.0 mg $Pt(acac)_2$, 20 mg AA and 28 mg dodecyl trimethyl ammonium bromide was dissolved in 12 mL Teflonlined autoclave containing 4.9 mL DMF. Adding 1.5 mL 0.25 M $Cu(acac)_2$ (dissolved in DMF) in the mixed solution. The resulting mixture was magnetically stirred at room temperature for 20 min and heated at 180 °C for 24 hours. The as obtained product was centrifuged three times at 10000 rpm for 20 min with ethanol, and the final product was stored in 5 mL ethanol solution.

Synthesis of H-PtCu/Pt_L OHs

The S-PtCuCo OHs solution (1 mL) was added to a 3-neck flask containing 5 mL DMF and ultrasonic mixed for 1 min, At the same time, 40 μL of concentrated

HNO_3 solution were rapidly added to the obtained mixture and heated continuously heated for 40 min under magnetic stirring at 70 °C. The as obtained product was centrifuged three times at 10000 rpm for 15 min with ethanol, then dispersed in 2 mL ethanol.

Structural characterization

The shape and size of samples were analysed by transmission electron microscope (TEM; JEM-1400 Flash at 120KV) and high-angle annular dark-field scanning TEM (HAADF-STEM; FEI Tecnai G2 F20 S-Twin HRTEM operating at 200 kV). The inductively coupled plasma optical emission spectrometry (ICP-OES) (Thermo Fisher Scientific, iCAP 7200) was used to analyze composition of samples. The X-ray diffraction (XRD) patterns of the samples were recorded on a Bruker D8 Advance X-ray powder diffractometer with Cu Kα radiation (λ=1.5418 Å) and graphite monochromator (40 KV, 40 mA). X-ray photoelectron spectroscopy (XPS) measurements were performed using AlK_a X-ray radiation (1486.6 eV) for excitation at 150 W (Thermo Fisher Scientific, USA).

Estimation of the alloy extent from XRD

The alloy extent is estimated by the variation of the lattice constant a/a_0. The alloy extent x can be obtained by the following equation:

$$\frac{x(1 - r_{Cu})}{r_{Pt}} = 1 - \frac{a}{a_0}$$

Where r_{Cu} and r_{Pt} are the atomic radius of Cu and Pt, respectively, a is the lattice constant of the catalyst, and a_0 is the lattice constant of pure Pt (that is, 3.923 Å; JCPDS no. 04-0802).

The computing method of d-band centers

The d-band centers of corresponding Pt nanocrystal and commercial Pt black were calculated from the following equation based on the valence band spectra:

$$d \text{ - band center } = - \int_{-1eV}^{8eV} [\text{binding energy}(E)\text{intensity}(E)]/\text{intensity}(E)dE$$

Electrochemical In Situ FTIR Spectra Measurements

The measurement of electrochemical in situ Fourier transform infrared (in situ FTIR) reflection spectroscopy was conducted on a Nicolet-iS50 FT-IR spectrometer containing a liquid-nitrogen-cooled MCT-A detector, at a spectral resolution of 8 cm^{-1}. The species (absorbed and dissolved) were measured on a thin layer (<10 μm) toward the working electrode and CaF$_2$ window for in situ FTIR. Multi-stepped FTIR spectroscopy (MS-FTIR) was utilized to collect spectra in 0.1 M HClO$_4$ + 0.5 M CH$_3$OH electrolyte from 0.09 to 1.19 V (vs. RHE) at 0.1 V intervals. The relative change in reflectivity (ΔR/R) of spectra was calculated by the following equation:

$$\Delta R/R = (R(E_S) - R(E_R))/R(E_R)$$

Where R(E$_S$) and R(E$_R$) are single-beam spectra collected at the sample potential E$_S$ and reference potential E$_R$.

Measurements of ORR performance

Electrochemical experiments were carried out in a standard three-electrode cell at room temperature controlled by CHI 760E electrochemical analyzer (CHI Instruments, Shanghai, Chenhua Co. Ltd.). The super pure water (18.25 MΩ cm) purified through a Milli-Q Lab system (Nihon Millipore Ltd.) was used as solvent. The working electrode is a glassy carbon (GC, Φ=5 mm, 0.196 cm^2) electrode embedded into a Teflon holder. Before the electrochemical test, the GC electrode was mechanically polished using successively alumina powder of size 1.5, 1.0 and 0.05 μm, and use ultrapure water cleaned in an ultrasonic bath. The suspension of catalysts was spread on the GC electrode. The Pt loading on the GC electrode of Pt/C, H-PtCu/Pt$_L$ OHs/C were 7.66 μg cm^{-2}, 7.5 μg cm^{-2}. As soon as the electrode was dried under infrared lamp, 2.5 μL Nafion solution (0.1 wt %) was coated onto the electrode surface. The cyclic voltammograms (CVs) were obtained in nitrogen-saturated 0.1 M HClO$_4$ solution, and the potential was scanned from 0.04 to 1.19 V (vs. RHE.) at a scan rate of 50 mV s^{-1}. Electrochemical experiments of ORR were performed using a glassy carbon

rotating disk electrode (RDE) (PINE, USA). An Ag/AgCl electrode and a graphite rod were used as the reference and counter electrode, respectively. The ORR measurements were conducted at room temperature in 0.1 M HClO$_4$ solutions after a flow of O$_2$ for a half hour until saturated, then using a glassy carbon RDE at a rotation rate of 1600 rpm with a scan rate of 10 mV s^{-1}. The accelerated durability tests were carried out in O$_2$-saturated 0.1 M HClO$_4$ solution by applying cyclic potential sweeps between 0.6 and 1.1 V (vs. RHE) at a sweep rate of 100 mV s^{-1}.

Rotating ring-disk electrode (RRDE) voltammetry

For the RRDE measurements, an RRDE with glassy carbon as the disk electrode (d=5.61 mm) and Pt as the ring electrode (Pine, collection efficiency=37%) was used as the working electrode. An Ag/AgCl electrode and a graphite rod were used as the reference and counter electrode. The disk electrode was scanned in the same potential range as the RDE measurement at a rate of 10 mV s^{-1}. The fraction of HO$_2^-$ formed during the ORR was determined by the following equation:

$$H_2O_2 = \frac{200 \, (I_D)}{(I_D N + I_R)}$$

where I_D is the disk current, I_R is the ring current and N is the collection efficiency of the Pt ring. Accordingly, we can also deduce the electron transfer number (n) of ORR over different catalysts:

$$n = \frac{4I_D}{(I_D + I_R N)}$$

The computing method of ECSA

The ECSA of H-PtCu/Pt$_L$ OHs/C, S-PtCu OHs and commercial Pt/C were calculated by the following equation:

$$ECSA = Q_H/(210 \times Pt_m)$$

Q_H is the charge for Hupd adsorption determined using $Q_H = 0.5 \times Q$, Pt_m is associated with the loading of Pt on the work electrode, and 210 μC cm^{-2} is the charge required for the monolayer adsorption of hydrogen on the Pt surface.

CO stripping test

All samples were carried out firstly in the N_2-saturated 0.1 M $HClO_4$ solution to test from 0.04 to 1.19 V (vs. RHE) at a scan rate of 50 mV s^{-1}, then input CO until saturation and recorded the CO-stripping CVs.

Methanol Oxidation Reaction (MOR) performance

CV curves were recorded in the N_2-saturated 0.1 M $HClO_4$ solution or 0.1 M $HClO_4$ + 0.5 M CH_3OH solution, an Ag/AgCl electrode and a graphite rod were used as the reference counter electrode, respectively. The suspension of catalysts was spread on the GC electrode. And the potential was scanned from 0.04 to 1.19 V (vs. RHE) at a scan rate of 50 mV s^{-1}. Later, the current–time (j-t) test was performed at 0.1 V for 3600 s.

DMPEMFCs test

The catalyst inks ((both anode and cathode) were made by mixing the 12.8 mg H-$PtCu/Pt_L$ OHs/C with 500 μL water, 2.5 mL isopropanol, and 100 μL 5% Nafion solution. After sonication for 45 min, half of the ink was sprayed on the carbon paper (AvCard GDS2240, 1×1 cm^2) to obtain the cathode catalyst layer and the other half of the ink was dripped on the foam nickel (1×1 cm^2) for the anode catalyst layer. The precious metal (Pt) loading of the cathode and anode is 2 mg cm^{-2}, respectively. For comparison, commercial Pt/C (60 wt%) prepared cathode and anode catalysts under the same conditions. The proton exchange membrane (Nafion N115) was first immersed in 3 % H_2O_2 at 70 °C for 1 hour, then immersed in water for 2 hours, and finally immersed in 0.5 M H_2SO_4 solution for 2 hours, and stored in water at room temperature. Then, the anode catalyst layer, proton exchange membrane, and cathode catalyst layer were sandwiched using hotpressing at 70 °C and 1 MPa for 60 s. The polarization curves were measured using the fuel cell test system (850e, Scribner Associates Inc.). The anode fuel was 0.5 M H_2SO_4 + 1 M CH_3OH solution with an injection rate of 2 mL min^{-1}, the cathode gas was O_2, and the flow rate was 250 mL min^{-1}. The performance of the battery was carried out at 70 °C.
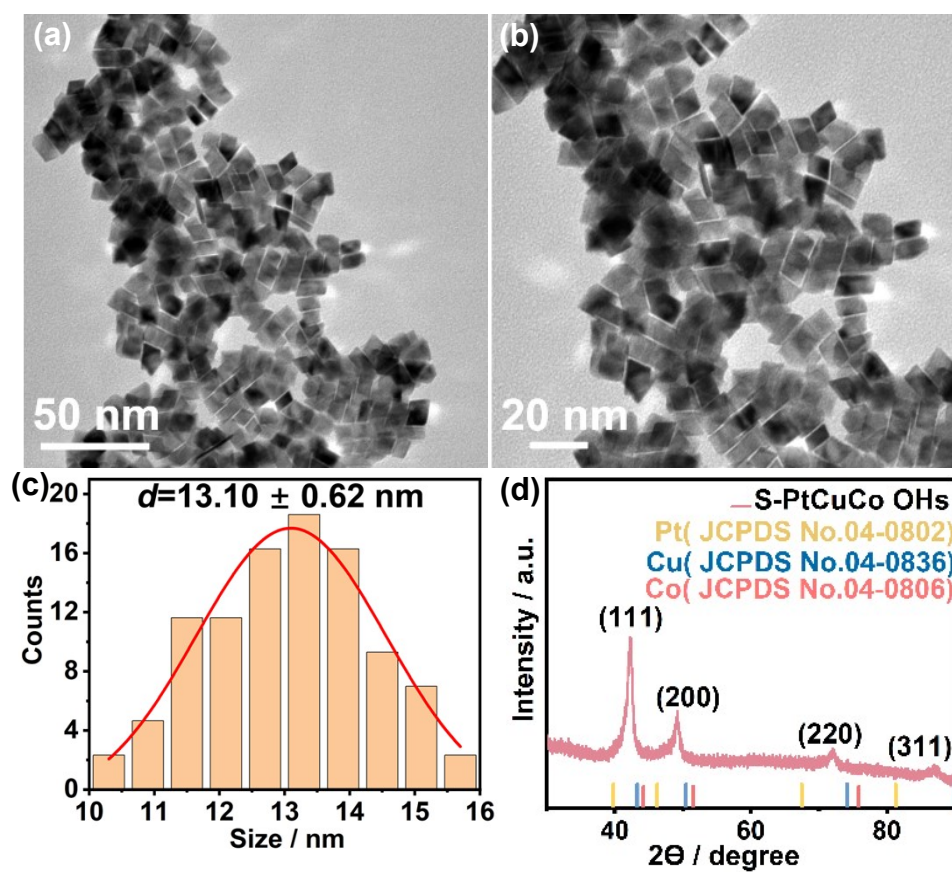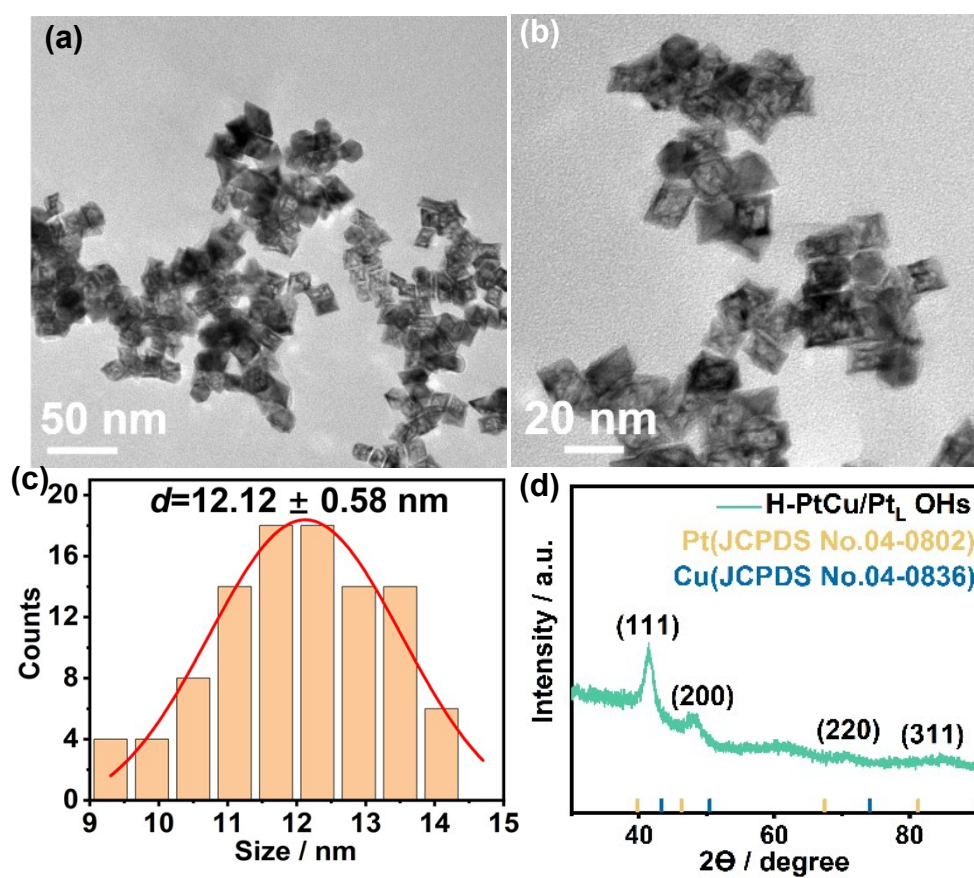
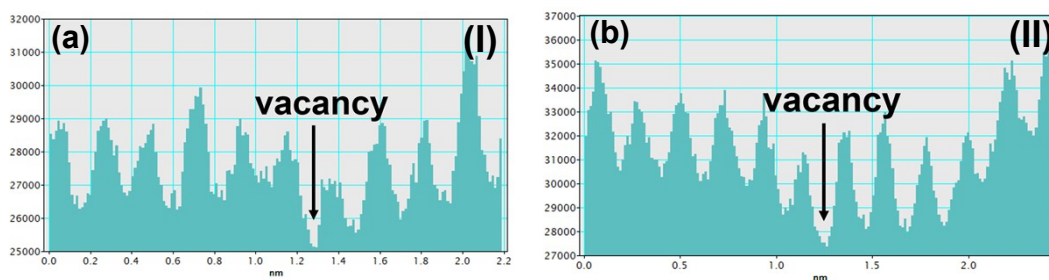**Fig.S1** (a, b) TEM images of alloyed S-PtCuCo OHs. (c) The column chart size of S-PtCuCo OHs.

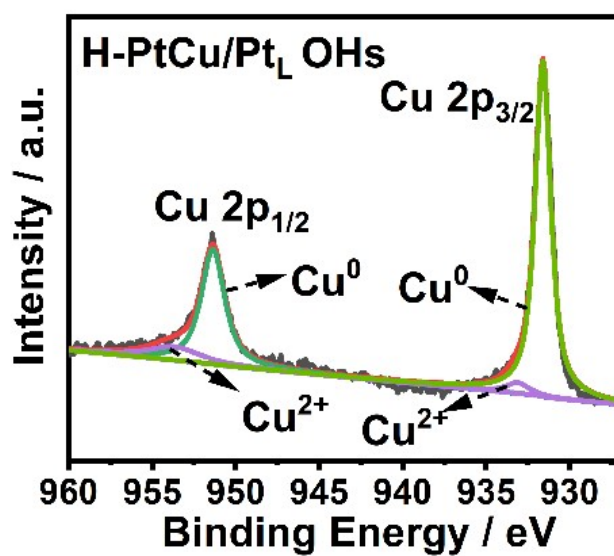(d) XRD spectra of S-PtCuCo OHs.
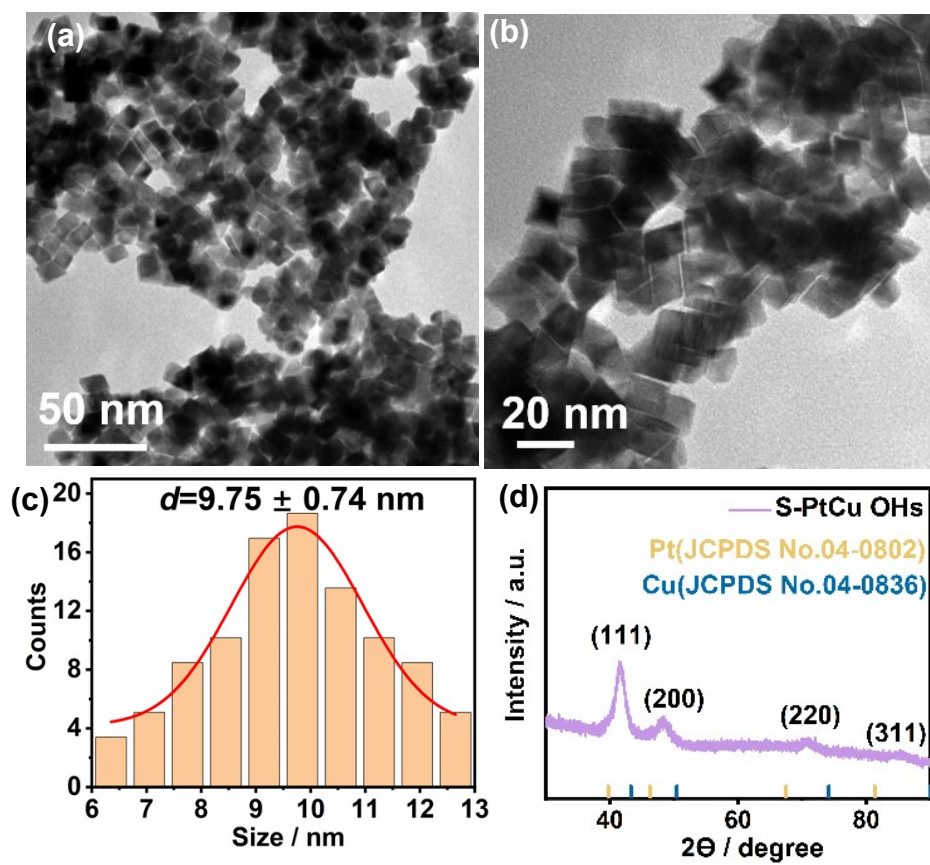
Fig. S2 (a, b) TEM images of alloyed S-PtCu OHs. (c) The column chart size of S-PtCu OHs. (d) XRD spectra of S-PtCu OHs.
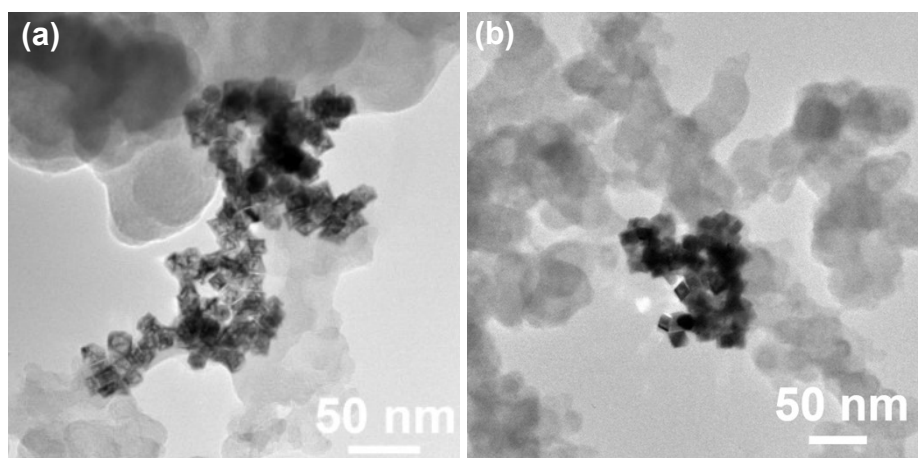
Fig. S3 (a, b) TEM images of H-PtCu/Pt$_L$ OHs. (c) The column chart size of H-PtCu/Pt$_L$ OHs. (d) XRD spectra of H-PtCu/Pt$_L$ OHs.

Fig. S4 (a) and (b) correspond to the atomic strength signal of I and II in Fig. 2c, respectively.

Fig. S5 XPS spectra Cu 2p of H-PtCu/Pt$_L$ OHs.

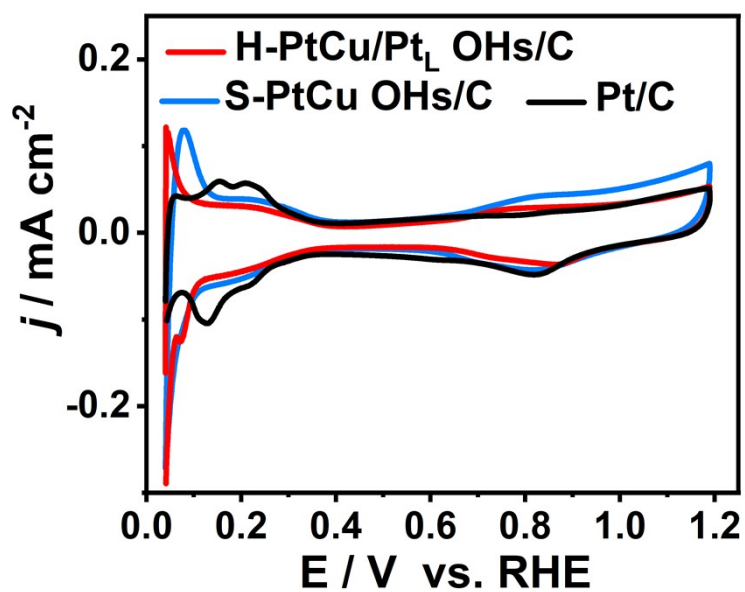**Fig. S6** (a) TEM images of H-PtCu/Pt$_L$ OHs/C. (b) TEM images of S-PtCu OHs/C.
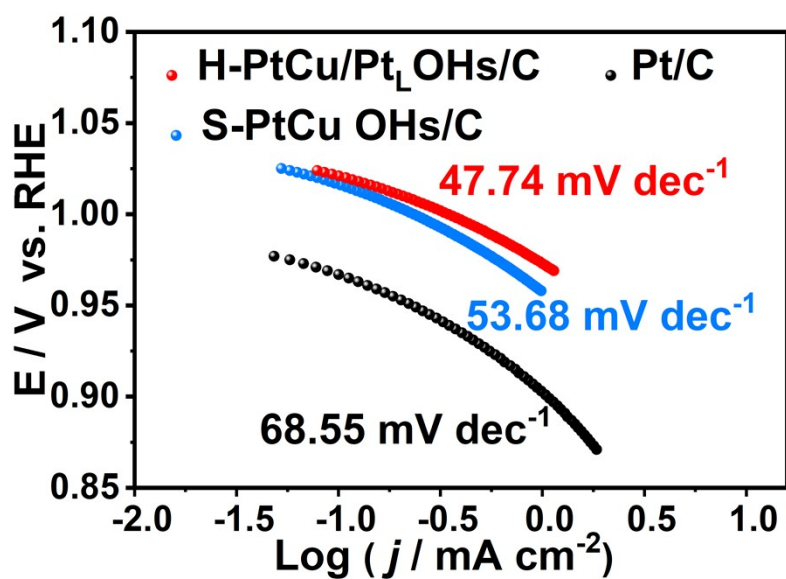
Fig. S7 CV curves of H-PtCu/Pt$_L$ OHs/C, S-PtCu OHs/C and Pt/C.
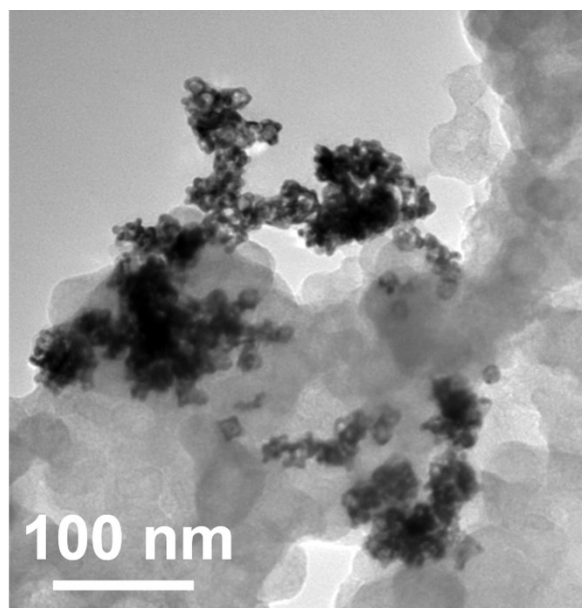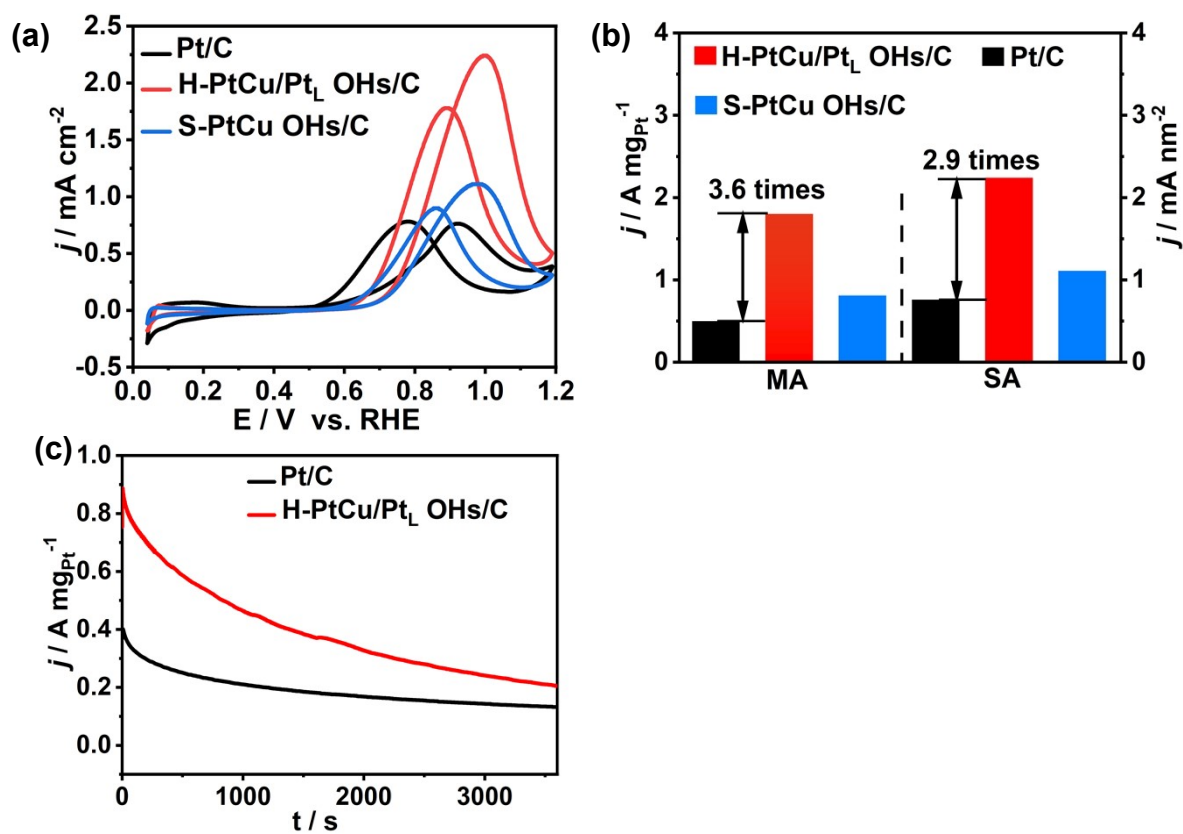
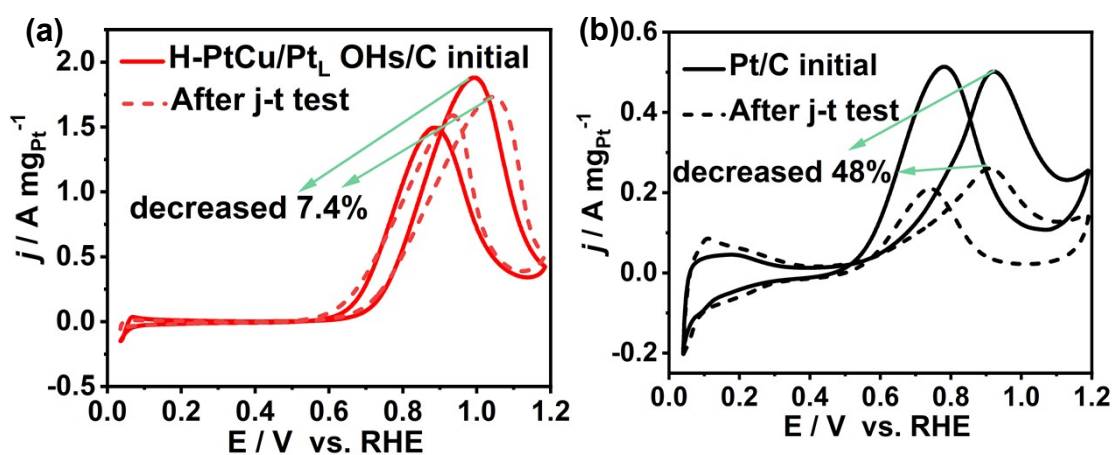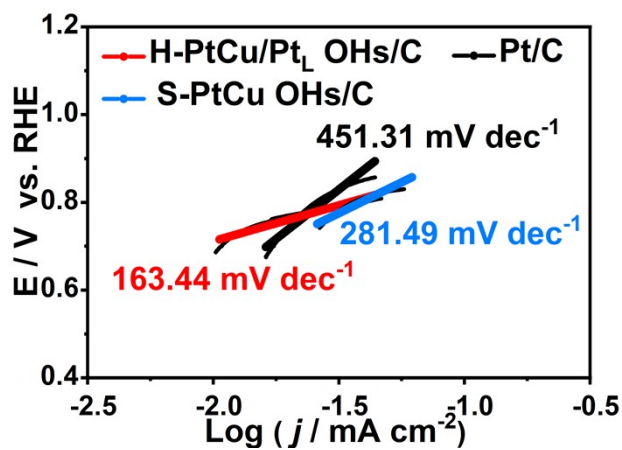**Fig. S8** The Tafel slope plots.

Fig. S9 TEM image of H-PtCu/Pt$_L$ OHs/C after 20K ADT.
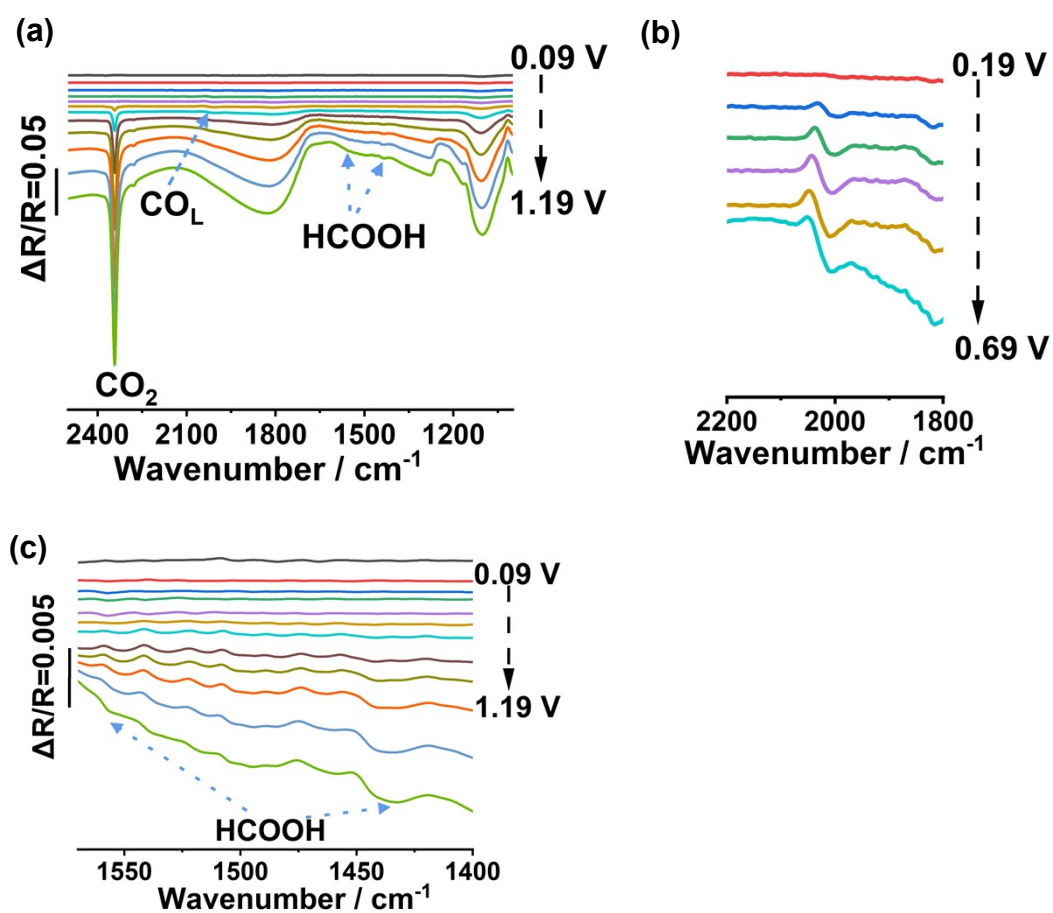
Fig. S10 (a) CV of the MOR specific activity. (b)Histogram of MA and SA. (b) j-t curves measured at 0. 84 V for 3600 s.

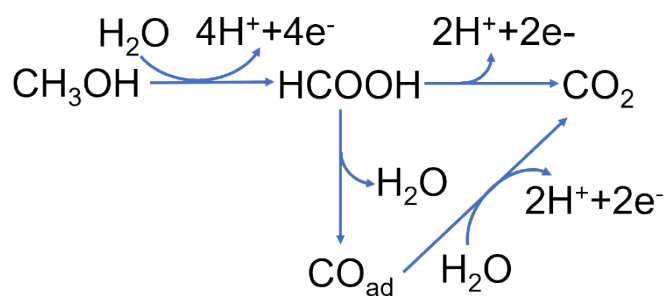**Fig. S11** MOR of (a) H-PtCu/PtL OHs/C, and (b) Pt/C before and after j-t.

Fig. S12 The Tafel slope diagram of CO stripping.

Fig. S13 In situ FTIR spectra of H-PtCu/Pt$_L$ OHs/C: (a) In situ FTIR total spectrum; (b) CO$_L$; (c)HCOOH.

Fig. S14 The Methanol oxidation reaction mechanism diagram of H-PtCu/Pt$_L$ OHs/C.

Table S1. XRD results of H-PtCu/Pt$_L$ OHs and S-PtCu OHs samples.

Catalysts	2θ/degree (111)	d$_{(111)}$ spacing (nm)	Lattice parameter (Å)	alloy extent (%)
H-PtCu/Pt$_L$ OHs	41.59	0.217	0.376	51.58
S-PtCu OHs	41.66	0.216	0.375	54.80
Pt (JCPDS No.04-0802)	39.80	0.226	0.392	

Table S2. Compositional analysis of as-prepared catalysts by ICP-OES measurements and XPS spectra measurements

Catalyst	Pt Atomic (%) (results from ICP-OES)	Cu Atomic (%) (results from ICP-OES)	Pt Atomic (%) (results from XPS spectra)	Cu Atomic (%) (results from XPS spectra)
H-PtCu/Pt$_L$ OHs	52	48	65.7	34.3

Table S3. Comparison of ORR catalytic activity at 0.9 V vs. RHE potential in 0.1 M $HClO_4$ electrolyte with catalysts reported in the literature

Catalysts	MA (A mg_{Pt}^{-1})	SA (mA cm^{-2})	References
H-PtCu/Pt$_L$ OHs/C	1.89	2.46	This work
PtCuNi/C	0.36	0.71	1
Pt$_2$Cu/C	0.51	-	2
PtCu NPs	0.92	1.94	3
PtCu NFs	0.82	1.24	4
Int-PtCuN/KB	1.15	1.18	5
Pd$_2$Cu@Pt/C	0.678	1.923	6
Mo$_{0.02}$-PtCu/C	1.61	2.84	7
PtCu$_3$Au$_{0.5}$ NWP	1.422	1.662	8
PtCu$_3$@Pt$_3$Cu@Pt	1.55	2.4	9
Pt$_3$Cu$_{97}$	1.85	5.78	10
Pd@PtCu/C	0.7	-	11
Pt$_{76}$Cu$_{24}$	0.466	1.273	12

Pd@Pt$_{1L}$/C	0.75	1.01	13
Pt octahedral nanocages	0.75	1.98	14

References

1. B. Li, Y. Ren, C. Lv, F. Gao, X. Zhang, X. Yang, L. Li, Z. Lu, X. Yu, *Int. J. Hydrogen Energ.,* 2023, **48**, 16286-16293.

2. X. Zhang, Z. An, Z. Xia, H. Li, X. Xu, S. Yu, S. Wang, G. Sun, *Appl. Surf. Sci.* 2023, **619**, 156663.

3. M. Sun, S. Gong, Z. Li, H. Huang, Y. Chen, Z. Niu, *ACS Nano.* 2023, **17**, 19421-19430.

4. M. Gong, D. Xiao, Z. Deng, R. Zhang, W. Xia, T. Zhao, X. Liu, T. Shen, Y. Hu, Y. Lu, X. Zhao, H. Xin, D. Wang, *Appl. Catal. B.,* 2021, **282**, 119617.

5. X. Zhao, H. Cheng, L. Song, L. Han, R. Zhang, G. Kwon, L. Ma, S. Ehrlich, A. Frenkel, J. Yang, K. Sasaki, H. Xin, *ACS Catal.,* 2020, **11,** 184-192.

6. W. Shi, A. Park, Y. Kwon, *Electroanal. Chem.,* 2022, **918**, 116451.

7. F. Wang, X. Wang, Z. Guo, J. Yu, H. Zhu, *Energy Fuels,* 2021, **35**, 3368-3375.

8. S. Zhang, H. Zhou, X. Liu, P. Tan, H. Liu, J. Pan, *J. Power Sources,* 2023, **567**, 232924.

9. Y. Liao, J. Li, S. Zhang, S. Chen, *Chinese J. Catal.,* 2021, **42**, 1108-1116.

10. M. Gatalo, F. Ruiz-Zepeda, N. Hodnik, G. Dražić, M. Bele, M. Gaberšček, *Nano Energy,* 2019, **63**, 103892.

11. G. Sievers, J. Bowen, V. Brüser, M. Arenz, *J. Power Sources,* 2019, **413**, 432-440.

12. M. Bao, I. Amiinu, T. Peng, W. Li, S. Liu, Z. Wang, Z. Pu, D. He, Y. Xiong, S. Mu, *ACS Energy Lett.,* 2018, **3**, 940-945.

13. M. Zhou, H. Wang, A. Elnabawy, Z. Hood, M. Chi, P. Xiao, Y. Zhang, M. Mavrikakis, Y. Xia, *Chem. Mater.,* 2019, **31**, 1370-1380.

14. L. Zhang, L. Roling, X. Wang, M. Vara, M. Chi, J. Liu, S. Choi, J. Park, J. Herron, Z. Xie, M. Mavrikais, Y. Xia, *Science,* 2015, **349**, 412-416.